Visible light active photocatalytic C-doped titanium dioxide films deposited via reactive pulsed DC magnetron co-sputtering: properties and photocatalytic activity

Marina Ratova[1*], Rachan Klaysri[1,2], Piyasan Praserthdam[2], Peter J. Kelly[1]

[1] Surface Engineering Group, School of Engineering, Manchester Metropolitan University, Manchester, M1 5GD, UK

[2] Centre of Excellence on Catalysis and Catalytic Reaction Engineering, Department of Chemical Engineering, Faculty of Engineering, Chulalongkorn University, Bangkok 10330, Thailand

* Corresponding author: M Ratova, School of Engineering, Manchester Metropolitan University, John Dalton Building, Chester Street, Manchester M1 5GD, UK, tel. +44 161 247 4648, e-mail address marina_ratova@hotmail.com

Abstract

Doping of TiO_2 with carbon is known to be an efficient method of enhancing visible light photocatalytic activity. The present work describes the deposition of carbon-doped titania coatings deposited by reactive magnetron co-sputtering of Ti and C targets. Undoped titania coatings were produced under similar deposition conditions for comparison purposes. Following deposition, all coatings were annealed in air at 873K for 30 min to develop the required crystalline structure; and then analysed with EDS, XRD, AFM, XPS and UV-visible spectrophotometry. A number of tests, including methylene blue and stearic acid decomposition tests, and photo-induced hydrophilicity measurements, were employed for the assessment of the photocatalytic properties of the C-doped and un-doped titanium dioxide coatings under UV and visible light irradiation. It was found that carbon-doped titania coatings significantly outperformed undoped titania when using both visible and UV irradiation. Similar trends were observed for other properties. While excessive carbon doping has been shown to have a negative effect on the photocatalytic properties of the titanium dioxide, overall, carbon doping

via reactive co-sputtering has been confirmed as an efficient method of photocatalytic property enhancement. This is due to a narrowing of the bandgap and to extended lifetimes of the photo-generated charge carriers.

1. Introduction

Photocatalytic materials are becoming increasingly popular as promising technologies for sustainable methods of surface, water and air decontamination [1, 2]. Titanium dioxide (or titania) is the most studied and widely used photocatalytic material due to such advantages as low cost, excellent chemical- and photo-stability and non-toxicity [3]. However, there are two major drawbacks with titania that are often reported as limiting the practical application of this material. Firstly, the relatively high band gap value (3.2 eV for anatase, reportedly the most photoactive phase of titanium dioxide) means that only the UV part of the solar spectrum can be utilised for photo-activation of TiO_2. Secondly, the fast recombination rate of the photo-generated charge carriers results in low quantum efficiency of titanium dioxide as a photocatalytic material. Various strategies are being extensively studied to extend the light absorption of TiO_2 into the visible region and to reduce the recombination of charge carriers, including photosensitization [4], semiconductor coupling [5, 6], doping with metallic [7, 8] and non-metallic elements [9, 10] (typically several atomic percent or lower), etc.

Doping of titania with p-block elements is generally seen as an efficient way of enhancing visible light photocatalytic activity, along with extending the lifetime of photogenerated charge carriers, as was first reported in the study published by Asahi and co-workers [11], who reported nitrogen doping of TiO_2 as a method of shifting the photoactivity towards the visible region. However, the efficiency of p-block element doping is still under debate, as insertion of dopant impurities may accelerate the charge carrier recombination rate [12]. Nevertheless, almost all p-

elements are reported to be used as TiO_2 dopants to date, including nitrogen [13, 14], carbon [15, 16], boron [17], sulphur [18] and phosphorus [19], as well as combination of several p-elements [20, 21] and simultaneous doping with metallic and non-metallic elements [9, 22, 23]. Although multiple computational and theoretical theories have been proposed to explain the effect of band gap narrowing as the result of p-block elements doping of titania, it is commonly accepted that such doping narrows the band gap of titanium dioxide due to mixing of the dopant p-states with the p-states of oxygen, forming the valence band of titanium dioxide [11]. While N-doping is by far the most studied approach, C-doping remains a less explored field to date, mainly due to difficulties in synthesizing carbon-doped titanium dioxide. Indeed, many chemical methods of synthesis, such as hydrothermal and solvothermal methods, flame oxidation or chemical vapour deposition, may require multiple process stages or the use of unsafe, unstable or expensive reagents [12]. Moreover, the use of different synthesis routes results in C-doped titania-based materials with different characteristics. In particular, depending on the preparation method, carbon atoms may be located in titania lattice in substitutional, interstitial or both positions, while the factors affecting this, as well as the effect of the dopant position on photocatalytic properties are not yet fully understood [12].

A number of methods are commonly used for the production of carbon-doped titanium dioxide materials, including chemical vapour deposition [24], sol-gel [16, 25, 26], hydrolysis [27], etc. Compared to the chemical methods mentioned above, pulsed reactive magnetron sputtering is recognised as one of the most convenient methods of depositing photocatalytic titanium dioxide-based coatings [28, 29]. It provides such advantages as relatively high deposition rates, precise control of the chemical composition of the film and use of non-hazardous solid sputtering targets. Moreover, the process is readily scalable and the substrate size can vary from mm^2 for laboratory-based work to several m^2 for industrial production [30]. Various methods can be used to introduce carbon for production of magnetron sputtered C-doped TiO_2 coatings. Using carbon dioxide as the reactive gas is probably the most studied technique of producing C-

doped TiO_2 via magnetron sputter deposition [31-33]. For this process, CO_2 can act a source of both carbon and oxygen [34]; alternatively O_2 can be introduced to the process as a second reactive gas [31, 33]. However, reactive magnetron co-sputtering typically provides an excellent and simple one-stage deposition method for depositing doped films, where the composition of materials and amount of dopant can be easily varied [7] by varying the power applied to co-sputtered targets. Nevertheless, reactive co-sputtering of titanium and carbon targets, remains a less studied method of doping TiO_2 films with carbon. Only a few publications have been found to date [35, 36], and no systematic study of the effect of sputtering conditions in such system on structural and photocatalytic properties of C-doped titania films has yet been reported.

Therefore, the aim of the present work is to deposit carbon-doped titania films using reactive magnetron co-sputtering of the host target (Ti) and dopant target (C), followed by a study of the structural, morphological and photocatalytic properties of these films. Carbon-doped coatings were compared to pure titania coatings deposited under otherwise identical conditions. This work was conducted as a part of series of the consecutive studies [33] aimed to study the effect of various carbon sources onto properties of C-doped titanium dioxide coatings.

2. Experimental

2.1. Deposition of the coatings

The coatings were deposited in a Teer Coatings Ltd. UDP350 sputtering rig from two 300 mm × 100 mm vertically opposed type II unbalanced planar magnetrons installed in a closed field configuration through the chamber walls. A solid, directly cooled titanium target (99.5% purity) was fitted on one of the magnetrons, and the carbon target (99.95% purity) was bonded to a copper backing plate and mounted on the other magnetron. The arrangement was similar to the one described in earlier work [37]. The magnetrons were driven in pulsed DC mode using a dual channel Advanced Energy Pinnacle Plus power supply; a pulse frequency of 100 kHz and duty of 50% (in synchronous mode) were used for all deposition runs. The titanium target was sputtered at a constant time-averaged power of 1kW for all runs, whereas the power applied to

the carbon target was varied from 100W to 200W to produce different carbon contents in the coatings. The reactive sputtering process was carried out in an argon / oxygen atmosphere at a pressure of 0.3 Pa. The flow of Ar was controlled with a mass-flow controller, while the oxygen flow was controlled by optical emission monitoring (OEM) using three different operating set points: 25%, 30% and 35% of the full metal signal (FMS) set points were selected (as compared to 15% used in earlier works to produce fully stoichiometric TiO_2 [7]) to create oxygen deficiencies in order to promote incorporation of carbon into the coatings, as titanium preferentially reacts with oxygen. All coatings were deposited onto soda-lime glass substrates, pre-cleaned in propanol prior to deposition and mounted onto a rotatable electrically floating substrate holder at 10 cm distance from the magnetrons. The rotation speed was set at 10 rpm for all deposition runs. Undoped titania coatings were additionally deposited for comparison purposes using the same optical emission set points; an overview of the deposition conditions is given in the Table 1. The deposition time for each reactive sputtering run was 2 h. The coatings were post-deposition annealed for 30 min at 873K in air for crystal structure development and then allowed to cool gradually in air for 10-12h to avoid the formation of thermal stresses in the coatings.

2.2. Characterisation of the coatings

The thickness of the coatings was measured by surface profilometry (Dektak^{TM}) and verified with 3D optical profilometry (Zemetrics 3D). The crystallography of the coatings was studied with Raman spectroscopy (Renishaw Invia, 514 nm laser) and X-ray diffraction (XRD) (Panalytical Xpert powder with CuKα1 radiation at 0.154 nm in grazing incidence mode at 3° over a scan range from 20° to 70° 2θ; the accelerating voltage and applied current were 40 kV and 30 mA, respectively). The elemental composition of the coatings was obtained by electron dispersive spectroscopy (EDS) (JEOL JSM-5410LV scanning microscope – where the calibration was performed with light element calibration standards and calculated ZAF factors were applied for calculation of the samples composition) and further verified with X-ray

5

photoelectron spectroscopy (XPS) – samples were sputter-cleaned prior to the analysis. The oxidation state information was obtained by X-ray photoelectron spectroscopy (XPS) (AMICUS photoelectron spectrometer equipped with an MgKa X-ray as a primary excitation source, and using Ag 3d as a reference binding energy at 368.2 eV). The surface areas of the coatings were determined with atomic force microscopy (AFM) (Veeco NanoScope IV MultiMode AFM). Band gap values of the coatings were calculated using the Tauc plot method [38], by plotting $(\alpha h v)^{1/2}$ as a function of hv and extrapolating the linear region to the abscissa (where α is the absorbance coefficient, h is Plank's constant, v is the frequency of vibration). Transmittance of the coatings for band gap calculations was measured with an Ocean Optics USB4000 UV-visible spectrometer.

2.3. Evaluation of photocatalytic activity

2.3.1. Methylene blue decomposition test

Methylene blue (MB) is an organic dye with molecular formula $C_{16}H_{18}ClN_3S$. Aqueous solutions of methylene blue have a bright blue colour with an absorbance peak at ca. 665 nm. Photocatalytic decomposition of methylene blue can be summarised with the following equation:

$$C_{16}H_{18}ClN_3S + 25.5 O_2 \xrightarrow[TiO_2, hv \geq BG]{} HCl + H_2SO_4 + 3HNO_3 + 16CO_2 + 6H_2O \qquad (1)$$
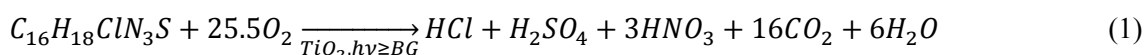
Changes in the absorbance peak height were used as a means of monitoring the concentration of the dye and hence its degradation in contact with the photocatalyst. Detailed descriptions of the test and a schematic representation of the testing setup are given elsewhere [9, 28, 37]. Prior to the test, samples of the same geometrical size (2.5×1.5 cm^2) were immersed into 40 ml of conditioning solution of the MB dye in the dark for a total time of 30 min to reach adsorption-desorption equilibrium. The sample was then withdrawn from the conditioning solution and immersed into 40 ml of testing solution with continuous magnetic stirring, while being irradiated with either UV or visible light for a total time of 1h. The concentrations of both

conditioning and testing MB solutions were 1.5 µmol/l (all reagents were purchased from Sigma-Aldrich, unless stated otherwise); these concentrations were pre-defined experimentally to detect the photocatalytic responses of all samples in a 1-hour experiment. An Ocean Optics USB4000 spectrometer was used to continuously measure the absorbance peak height at 665 nm. Each coating was tested both under UV and visible light; 2 × 15 W 352 nm Sankyo Denki BLB lamps were used as the UV light source, while visible light was simulated by combining a fluorescent light source (2 × 15 W Ushio fluorescent lamps) with a Knight Optical 395 nm long pass UV filter. The emission spectra of the UV and visible light sources used are given in the Figure 1.
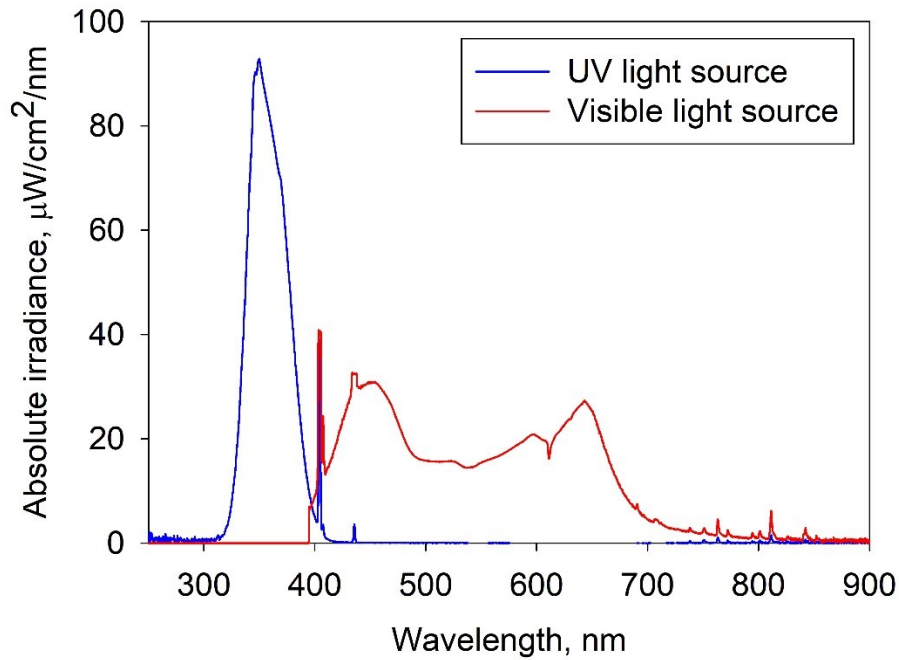

Figure 1. Emission spectra of UV and visible light sources used for the photocatalytic testing

According to the Lambert – Beer law, the concentration of the dye is proportional to the absorbance decay. Photocatalytic methylene blue decomposition can be approximated to first order kinetics:

$$ln\frac{c_0}{c} = k_a t \qquad (2)$$

Where C_0 and C are the concentrations of MB solution at time 0 and time t of the experiment, respectively; k_a is the first order reaction constant; t is the time. Therefore, the apparent first order reaction constant was used here for quantitative characterisation of the MB decomposition process; it was determined as the gradient of the plot $\ln(A_0/A)$ vs time (where A_0 and A are the peak absorbance values of MB at time 0 and time of the experiment, respectively). A series of reference tests was performed prior to the photocatalytic activity measurements, which included tests with blank samples (soda-lime glass of the same geometrical size) under each light source, as well as tests of each sample in dark conditions, to prove that solution decolourization was caused by a photocatalytic reaction. As none of the reference tests showed more than 1% peak height decay in a 1h experiment, their effect was neglected in further calculations.

2.3.2. Stearic acid decomposition test

As the reliability of the dye degradation test under visible light is frequently questioned in research papers [39], a stearic acid (SA) decomposition test was used to verify the MB degradation results.

Stearic acid decomposition as a function of time is frequently used for the assessment of photocatalytic activity [40]. The decomposition process can be summarised with the following equation:

$$CH_3(CH_2)_{16}COOH + 26O_2 \xrightarrow[TiO2,\ hv \geq BG]{} 18CO_2 + 18H_2O \tag{3}$$
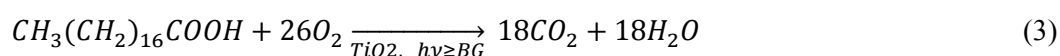
A 0.1M solution of stearic acid in acetone was used for the test. Samples of the same geometrical size (1.5×2.5 cm^2) were spin-coated with 0.5 ml of stearic acid solution using an Osilla spin coater at 1000 rpm speed for a total time of 30 sec. After spin-coating the samples were stored in the dark for 1h to allow acetone evaporation from the surface. Stearic acid has strong absorption peaks at 2958, 2923 and 2853 cm^{-1} [41], therefore destruction of the stearic acid was monitored by Fourier transform infrared spectroscopy (FTIR) (Perkin Elmer IR spectrometer) in the range 2700-3000 cm^{-1} every 24h. Infrared spectra were collected in

absorbance mode; the amount of stearic acid on the surface of sample is proportional to the integrated area under the corresponding FTIR spectrum. The light sources used for irradiation of these samples were identical to the light sources used for the MB decomposition tests. All photocatalytic experiments were conducted in triplicate to ensure reproducibility.

2.3.3. Photoinduced hydrophilicity measurements

It is generally accepted that the superhydrophilic properties of TiO_2 develop when the material is irradiated with light with an energy higher than the material band gap value. This effect supposedly originates from water adsorption on photogenerated oxygen vacancies on the photocatalyst surface [42]. This phenomenon only lasts for a certain period of time, and the surface returns to its original state after being stored in the dark [43]. Therefore, photoinduced hydrophilicity measurements are frequently used as an indication of the photocatalytic efficiency of a material. Here water droplet contact angle measurements were made to determine the wettability change of pure and C-doped TiO_2 samples under visible light irradiation. Prior to the photoinduced hydrophilicity measurements, samples were stored in the dark for 24h. The films were irradiated with visible light, and static water droplet contact angles (WCA) were measured with a Theta Lite optical tensiometer every 10 minutes for a total time of 30 min. The average contact angles values were obtained by taking a mean value of 5 measurements across the sample surface.

3. Results

3.1. Coatings overview

The overview of the coatings, including deposition conditions, thickness and elemental composition after annealing at 873K is given in the Table 1. Elemental content of the coatings was estimated with EDX and further verified later with XPS. For both undoped and C-doped titania coatings, the difference in thickness between coatings deposited at OEM set points of 25 and 30% was minimal, while the coatings deposited at 35% set point were considerably thicker

in all cases, which is indicative of the greater degree of poisoning of the Ti target at the lower

OEM turndown signals (greater oxygen flow rates). As expected, for undoped coatings the

OEM set point of 25% resulted in production of TiO_2 film with Ti : O ratios close to the

stoichiometric 1 : 2 [7]; reduction of oxygen flow at higher OEM signals resulted in an increase

of the Ti : O ratio. However, for all of the C-doped coatings, the ratio of Ti : O remained quite

stable, and the variations of OEM set point resulted in different carbon contents. However, the

interactions occurring between the power applied to the carbon target and OEM settings are not

yet fully understood. As can be seen from the results presented in the Table 1, increasing the

power applied to carbon target reflected in higher carbon content in the coatings.

Table 1. Deposition conditions, compositional properties and thickness of undoped and C-doped titania films after annealing at 873K

Sample ID	O$_2$ OEM set point, %FMS	Power applied to C target, W	Coating thickness, nm	Ti content, at. %	O content, at. %	C content, at. %
T25	25	-	490	34.9	65.1	-
T30	30	-	510	40.9	59.1	-
T35	35	-	600	40.2	59.8	-
T25C100	25	100	660	33.8	60.3	5.9
T30C100	30	100	670	33.6	60.9	5.5
T35C100	35	100	760	33.9	58.7	7.4
T25C200	25	200	660	30.9	62.6	6.6
T30C200	30	200	730	32	60.6	7.3
T35C200	35	200	850	33.9	57.0	9.1

Key: Txx – titania only coatings; TxxCyyy – C-doped titania coatings

3.2. XRD results

The crystallographic structures of the undoped and C-doped titania coatings were characterised by X-ray diffraction. Based on the XRD results, all the as-deposited coatings were characterised with amorphous or weakly crystalline microstructures. Therefore, they were annealed in air at 873K to promote development of the crystal structure (the annealing temperature was defined experimentally to ensure that all of the studied coatings were crystalline). The XRD patterns of the annealed coatings are presented in Figure 2. The data were divided into three parts for ease of comparison, based on the oxygen flow set point. It can be seen that undoped titania coatings (samples T25, T30 and T35) exhibited only anatase crystal structure peaks identified by the crystallographic card number 96-900-8215, with major anatase peaks found at 2θ angles of 25.3°, 37.8°, 48.0°, 55.0° and 62.6°. Unlike undoped TiO_2, coatings co-deposited using titanium and carbon targets were characterised with mixed phase structures, where rutile and brookite peaks could be seen on the patterns, as well as the anatase peaks (crystallographic cards for rutile and brookite phases were 96-900-4145 and 96-900-4138, respectively). For all films studied, the anatase (101) peak was the most pronounced. No additional peaks besides those corresponding to different titania phases were found in any of the XRD patterns obtained.

The crystallite sizes were calculated using the Scherrer formula from the anatase (101) peaks at 25.3° 2θ:

$$D = \frac{0.89 \times \lambda}{\beta \times cos\theta} \tag{4}$$

Where D is the crystallite size (nm), λ is the CuKα wavelength (0.154 nm), β is the full width at half maximum intensity of the peak (radians), and θ is the corresponding diffraction angle. Prior to calculation of the crystallite sizes, Kα2 and instrumental broadening effects were removed. The calculated sizes of the crystallites ranged from 13 to 21 nm (given in Table 2), and C-doped films were generally characterised with larger crystallites, compared to undoped TiO_2 films.
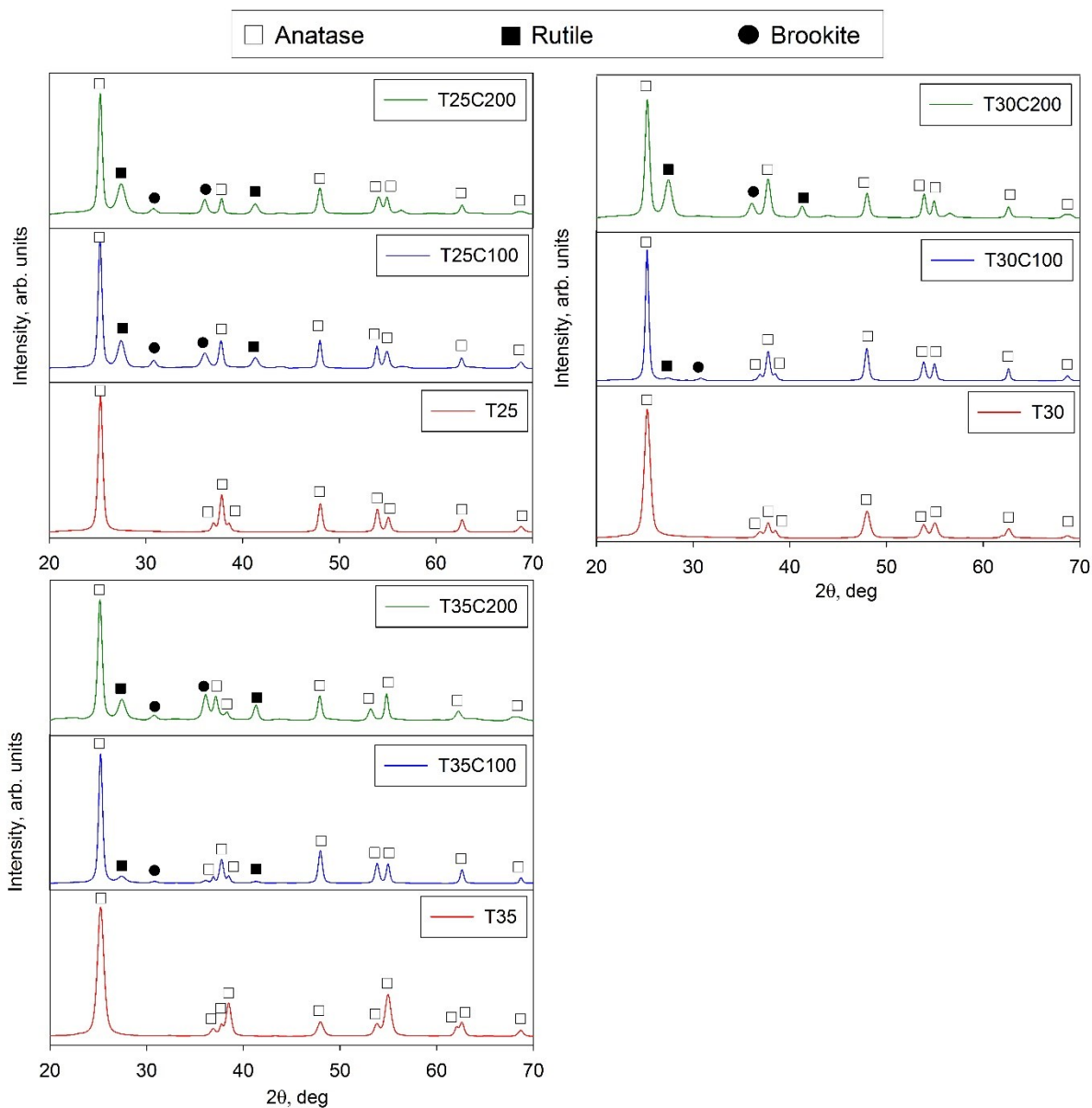
Figure 2. XRD patterns of C-doped and undoped TiO₂ coatings deposited on glass substrates and annealed at 873K.

Table 2. Phase, optical properties and surface areas of C-doped and undoped TiO₂ films annealed at 873K

Sample ID	Crystal phase	Crystallite size, nm	Average	Band gap, eV	Absorption	Atomic percentage of	Surface area, μm^2	Surface roughness, nm

			visible light transmittance (%)		edge, nm	C-doping, %		
T25	Anatase	15	80.2	3.22	385	-	902	5.6
T30	Anatase	13	80.4	3.20	387	-	903	5.9
T35	Anatase	13	81.0	3.18	390	-	909	6.2
T25C100	Anatase / rutile brookite	17	81.5	3.14	395	0.59	901	5.4
T30C100	Anatase / rutile brookite	20	82.1	3.13	396	0.54	903	6.3
T35C100	Anatase / rutile brookite	20	82.3	3.13	397	0.55	902	5.3
T25C200	Anatase / rutile brookite	17	82.3	3.12	397	1.26	901	3.2
T30C200	Anatase / rutile	20	84.8	3.10	400	1.31	901	4.2

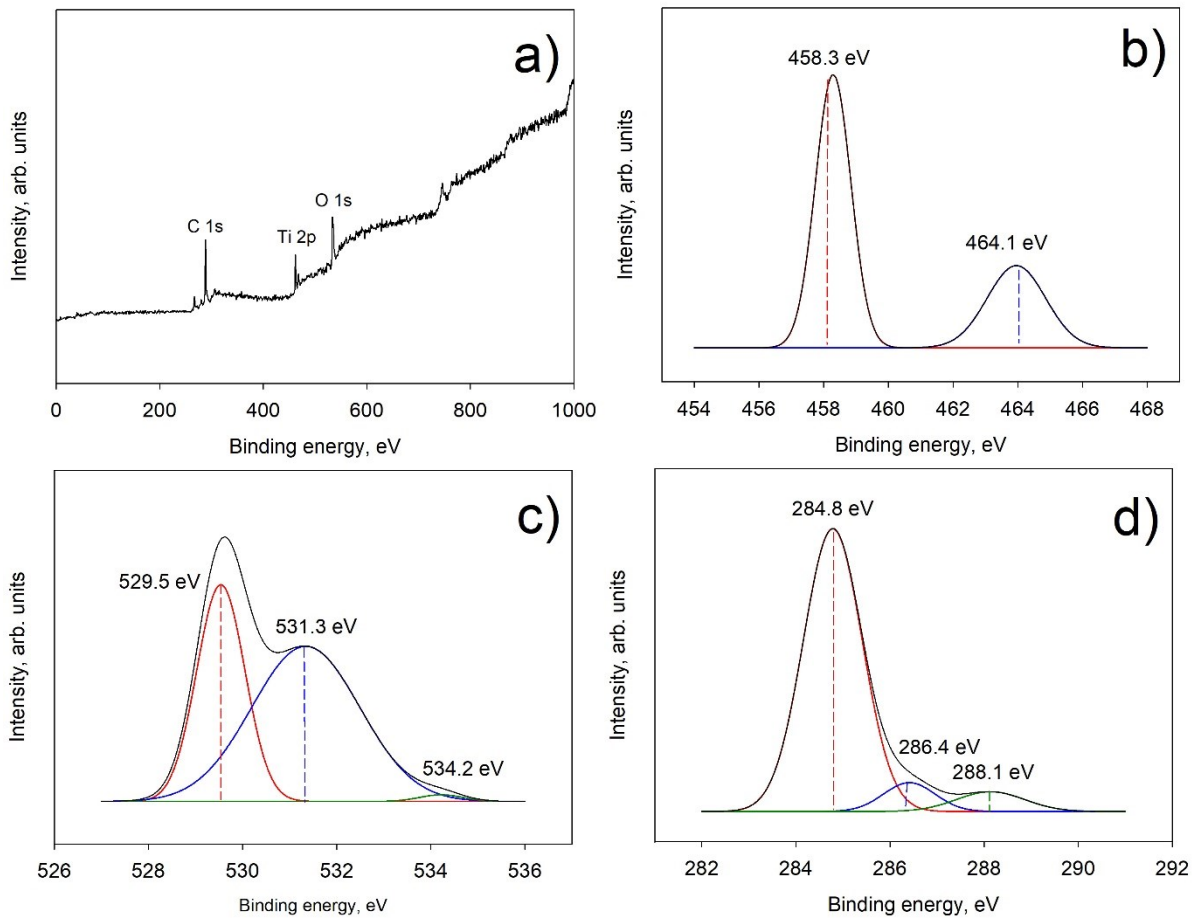|	brookit e							
T35C20 0	Anatase / rutile brookit e	21	48.6	2.97	417	1.76	905	9.9

3.3. XPS results

Figure 3. XPS results of sample T25C100: a) Survey spectrum; b) Ti 2p spectrum; c) O 1s

spectrum; d) C 1s spectrum

Surface composition and chemical states of the elements were studied with X-ray photoelectron spectroscopy (XPS). Examples of the XPS results (for coating T25C100) are given in the Figure 3. The survey spectrum is shown in Figure 3a; two of the strongest peaks of the spectrum at 527 and 456 eV can be assigned to O 1s and Ti 2p excitations, respectively. An additional peak that belongs to C 1s is found at 284 eV. High resolution XPS spectra of Ti 2p, O 1s and C 1s are given in the Figures 3b-d, respectively. On the high resolution spectrum of Ti 2p (Figure 3b), the peak positioned at 458.3 eV corresponds to Ti $2p_{3/2}$, while the peak at 464.1 eV can be assigned to Ti $2p_{1/2}$ (both observed peaks fit well with the positions of Ti in TiO_2). No significant differences can be observed between the Ti 2p XPS spectra of C-doped and undoped titania samples. Figure 3c shows high resolution spectrum of O 1s binding energies. Three peaks can be clearly distinguished after curve fitting, at 529.5, 531.3 and 534.2 eV, that can be assigned to Ti-O bonds, C-O bonds and organic C-O bonds, respectively. The high resolution spectrum of C 1s (Figure 3d) has three peaks; the peak at 284.8 eV is typically assigned to elemental carbon, while two peaks at 286.4 and 288.1 eV can be attributed to the oxygen bound species, C-O and Ti-C-O, respectively [44], suggesting that in this case carbon was incorporated into the titania lattice by substituting some of Ti atoms [25]. An absence of peaks below 284.8 eV is evidence of the fact that no substitution of O atoms by C atoms occurred [24]. The atomic percentage of carbon substituting was estimated using the relative areas of the of 288.4 eV peaks; these data are given in the Table 2.

3.4. Films morphology (AFM results)
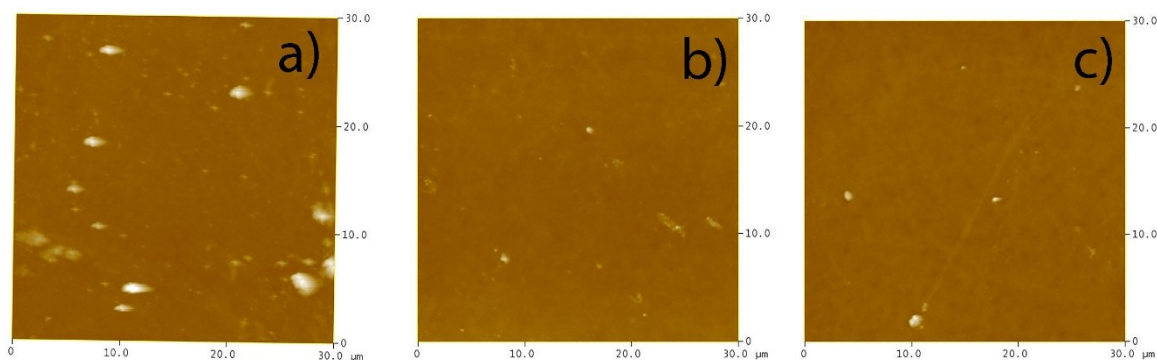
Figure 4. Examples of AFM images for undoped and C-doped titania coatings deposited at an

OEM set point of 25% FMS: a) T25; b) T25C100; c) T25C200

Atomic force microscopy was used to study the morphological properties of the coatings.

Examples of AFM images for samples deposited at an OEM set point of 25% FMS are shown in

Figure 4. Values of surface roughness (R_a) and surface area (S_a) obtained by AFM are given in

Table 2. It is evident that all coatings studied were relatively smooth. Neither variations of the

oxygen flow nor the power applied to the carbon target had any significant effect on the values

of the coating surface parameters. It should be noted, though, that surface roughness of coating

T35C200 was slightly higher, as compared to the rest of the array, however, this coating was

also considerably thicker.

3.5. Band gap calculation

Optical band gap values of the undoped and C-doped TiO_2 coatings were estimated using the

classical Tauc plot method for crystalline semiconductors, as described earlier in the

Experimental section. Figure 5 shows examples of band gap calculations for samples deposited

at an OEM set point of 25% FMS (samples T25, T25C100 and T25C200). The calculated values

of the band gaps for all coatings studied within this work are given in the Table 2. It is evident

that the light absorption characteristics of magnetron-sputtered TiO_2 films were significantly

affected by carbon doping. While the band gap values of pure titania films ranged from 3.22 to

3.18 eV (as expected for anatase films), the absorption edges were all red-shifted for the C-

doped coatings (up to 2.97 eV for sample T35C200). It should be noted that for all samples
except T35C200 the absorption edge shift did not result in a change in the value of average
spectral transmittance in the visible region (Table 2). However, this coating was also noticeably
thicker than the others. The band gap data are in good agreement with the literature information,
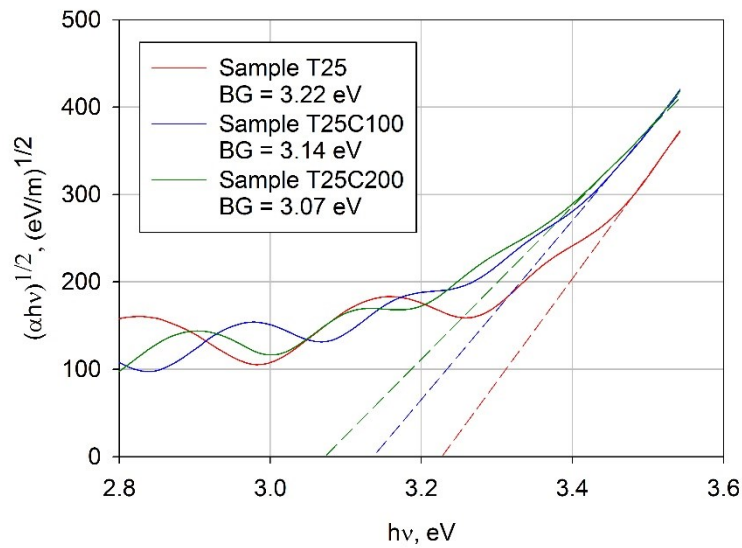where the value of anatase titania is typically reported to be around 3.2 eV.

Figure 5. Examples of band gap calculations for samples deposited at an oxygen flow set point

of 25% FMS

3.6. Photocatalytic activity measurements

Table 3. Results of photocatalytic tests of C-doped and undoped TiO$_2$ coatings annealed at

873K

Sample ID	MB UV $k_a \times 10^5$, s^{-1}	MB vis $k_a \times 10^5$, s^{-1}	SA UV, k_a, A cm^{-1} h^{-1}	SA vis k_a, A cm^{-1} h^{-1}	R$_{WC}$, UV (1h)	R$_{WC}$, vis (1h)
T25	1.8	0.5	0.04	0	0.29	0.65
T30	1.4	0.9	0.02	0	0.26	0.70

T35	1.4	0.9	0.02	0.01	0.08	0.72
T25C100	2	1.3	0.15	0.05	0.09	0.25
T30C100	1.9	1.3	0.16	0.06	0.14	0.48
T35C100	1.8	1.5	0.17	0.05	0.17	0.55
T25C200	2.5	1.5	0.17	0.07	0.27	0.63
T30C200	2.5	1.4	0.14	0.05	0.17	0.45
T35C200	1.1	0.2	0.01	0	0.32	0.43

Key: MB UV – rate constant of MB degradation reaction under UV light; MB vis - rate constant of MB degradation reaction under visible light; SA UV – rate constant of stearic acid degradation reaction under UV light; SA vis – rate constant of stearic acid degradation reaction under visible light; R_{WC} UV - hydrophobic recovery rate under UV light; R_{WC} vis - hydrophobic recovery rate under visible light

3.6.1. Methylene blue decomposition test

Firstly, the photocatalytic properties of the coatings were assessed by monitoring the MB dye decomposition, both under UV and visible light sources. The calculated values of the reaction first order rate constants are given in Table 3 for a quantitative characterization of the dye photodegradation process. Some examples of MB degradation kinetics for samples deposited at an OEM set point of 25% FMS under UV and visible light are shown in the Figure 6. Unsurprisingly, undoped titania coatings were efficient photocatalysts under the UV light source, while under visible light their MB decomposition activity dropped significantly. Coatings T30 and T35 were more efficient under visible light, compared to T25, most likely due to their slightly lower band gap values. It is evident from the data in Table 3 that the photocatalytic activity of all the C-doped coatings (except T35C200) was superior to that of undoped titania, under either of the light sources used.
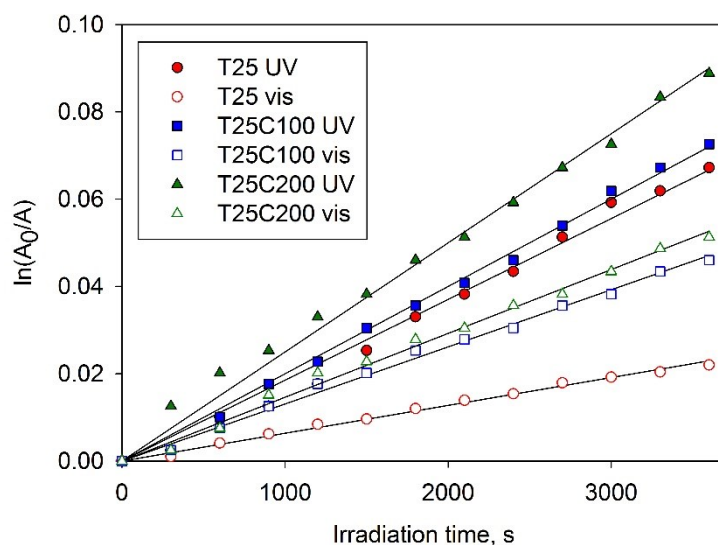
Figure 6. MB degradation kinetics under UV and visible light in contact with samples deposited at oxygen flow set point of 25% FMS

However, despite the fact that the MB decomposition test is one of the ISO-standardized tests for assessment of photocatalytic activity under UV light [45], the suitability of it for visible light activity assessment is often questioned [46]. This is due to the fact that the contribution of the dye-sensitised non-photocatalytic photobleaching of the reaction may be significant under visible light. Therefore, a number of other tests were used in this work to verify the photocatalytic activity of undoped and C-doped titania films.

3.6.2. Stearic acid decomposition test

Photocatalytic activities of reactively co-sputtered C-doped and undoped TiO_2 coatings were determined using the stearic acid decomposition test. Stearic acid is a frequently used photocatalytic test model pollutant, especially for assessing self-cleaning properties of photocatalytic coatings [40]. It is generally accepted that the stearic acid photocatalytic decomposition reaction pathway has no major intermediates, therefore it can be easily monitored through IR-observable species (SA disappearance or CO_2 generation). Figure 7

shows an example of infrared spectra that clearly illustrate photocatalytic-induced disappearance of stearic acid peaks as a function of irradiation time (sample T25, UV light).

Monitoring of SA IR peaks under UV and visible light illumination for a total time of 96h generated the plots presented in Figure 8. Additionally, for quantitative characterisation of the photocatalytic decomposition process, first order rate constants of stearic acid degradation were calculated and listed in Table 3. Control tests with SA films deposited onto pieces of uncoated soda-lime glass were carried out for both light sources used.
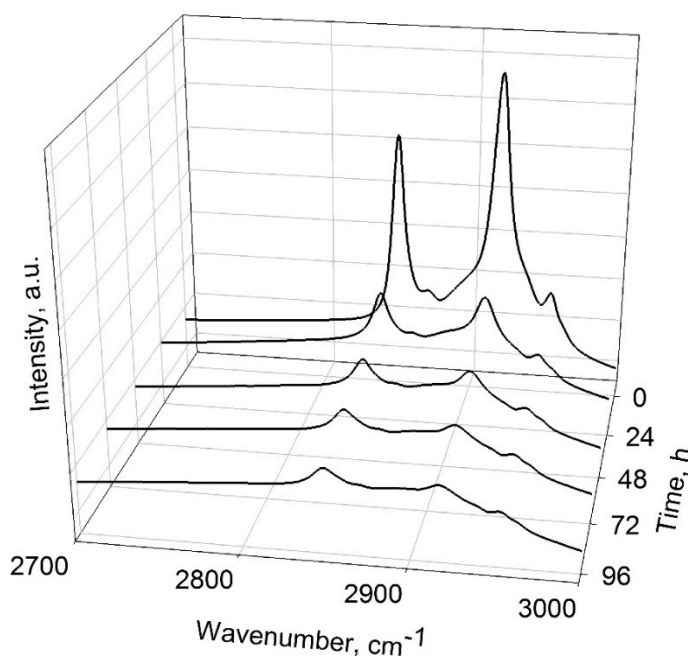
Figure 7. Examples of recorded FTIR spectra of stearic acid film as function of time on the surface of sample T25 irradiated with UV light
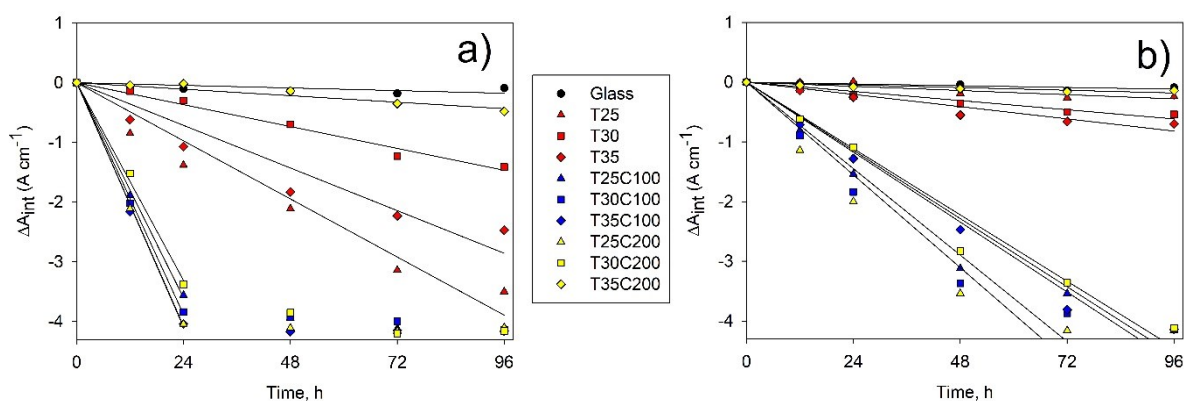
Figure 8. Plots of the integrated area changes of the FTIR spectra of the stearic acid peaks (3000 - 2700 cm^{-1}) for C-doped and undoped TiO$_2$ samples under: a) UV light irradiation; b) visible light irradiation

From the data presented in Figure 8, it is evident that stearic acid films were stable under both UV and visible light irradiation, as no significant peak reduction was detected on plain glass during each 96h experiment. Of the undoped titania coatings, sample T25 was characterised with the highest activity for SA decomposition under UV light. Under visible light illumination, the efficiency of all the undoped TiO$_2$ samples was very low, with T30 and T35 slightly outperforming T25, probably due to their slightly lower band gap values. It is clear that the photocatalytic activity of all C-doped samples, except T35C200, was higher than that of the pure titania samples. It should be noted that under UV illumination no stearic acid IR peaks could be seen for 5 out of 6 C-doped samples already after 24h, hence the reaction rate constants here were calculated here based just on 0h, 12h and 24h data points. Under the visible light source, full degradation of stearic acid (full disappearance of the IR peaks) was observed after 72h illumination for samples T35C100 and T25C200, and after 96h illumination for samples T25C100, T30C100 and T30C200. It is obvious that, similarly to the UV result, the activity of sample T35C200 was close to zero.

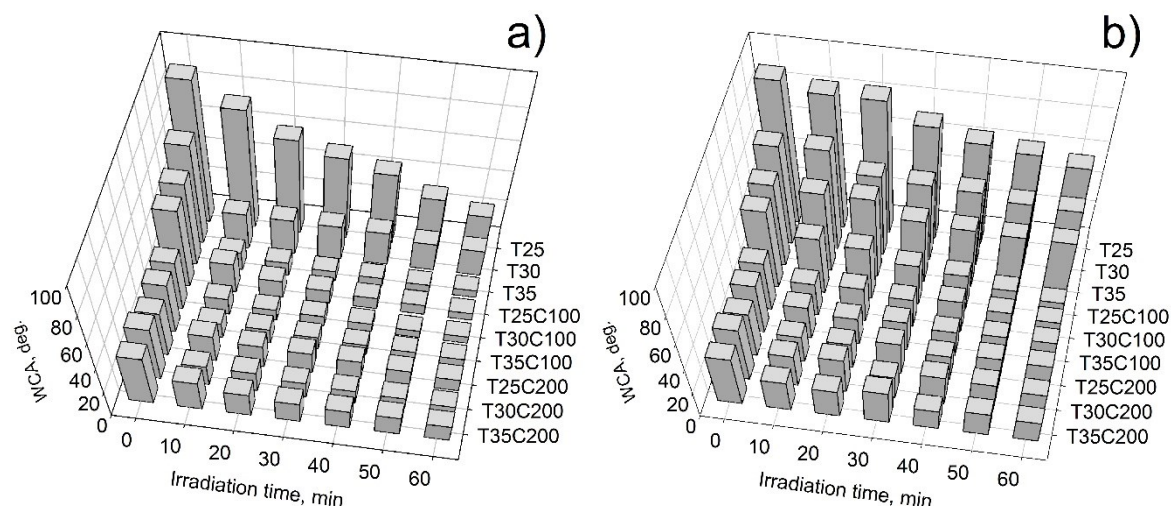### 3.6.3. Wettability (photoinduced hydrophilicity) measurements

21

Figure 9. Water droplet contact angles change as a function of irradiation time: a) UV light irradiation; b) visible light irradiation.

Water droplet contact angle measurements under UV and visible light were performed to study changes in sample wettability upon irradiation. The value of hydrophobic recovery rate (R_{WC}) was used for quantitative characterisation of photoinduced hydrophilicity. R_{WC} is typically defined as the ratio of WCA after irradiation to WCA of the same surface in the dark (prior to irradiation) [20]. Prior to irradiation initial water contact angle (WCA) measurements ranged from ca. 90 to 40°. The changes of water droplet contact angles as a function of UV / visible light irradiation over 1h period are depicted in the Figure 9. It is evident, that initial contact angles of undoped titania films were higher, compared to C-doped coatings. After 1h of UV light irradiation WCA of C-doped films dropped to 5-6° (superhydrophilic state); this number was slightly higher for undoped films, nevertheless all of the studied films under UV light irradiation exhibited a pronounced phenomenon of photoinduced hydrophilicity.

For visible light irradiation, it can be seen that the WCA of undoped titania samples remained relatively high after 1h of irradiation, while all of C-doped samples exhibited pronounced photoinduced hydrophilicity during 1h experiment, with values of WCA ca. 14-20° at the end of the experiment.

4. Discussion

Incorporation of carbon into the titania lattice is frequently reported to reduce the band gap [4], but the effect of the doping on photocatalytic properties depends significantly on the position of the impurity atom in the titania lattice, which in turn depends on the production method, etc. The present work confirms that the deposition of C-doped titania coatings by reactive magnetron co-sputtering is an efficient pathway to the production of visible light-active TiO_2-based photocatalysts.

It is known that titanium preferentially reacts with oxygen, therefore for incorporation of carbon atoms into the titania lattice, oxygen deficiencies were created by reducing the oxygen flow (achieved here by varying the optical emission set point value).

Judging from the XRD data, it is possible to conclude that the incorporation of carbon reduced the thermal stability of anatase for all C-containing coatings. Reduction of the anatase thermal stability after carbon doping is a known effect [16], which is typically explained by distortion of the lattice parameters as a result of dopant incorporation. Despite the fact that anatase is generally reported as the most photoactive phase of titanium dioxide, a number of studies have shown that mixed phase photocatalysts, with a small amount of rutile phase, often exhibit better photocatalytic properties, as compared to pure anatase ones [47]. The fact that the most used commercial photocatalyst, Degussa P25, contains ca. 80% of anatase and 20% rutile [48], supports this suggestion. Though the preferred ratio of anatase / rutile varies depending on the study, it is generally believed that polycrystallinity improves photocatalytic performance and the presence of the rutile phase plays a key role in separating electrons and holes and, therefore, slows down the recombination of photogenerated species [48].

Doping of titania with p-elements in general, and with carbon in particular, typically results in band gap narrowing [12]. Indeed, in the present work the value of the band gap of the coating with the highest content of carbon is 0.25 eV lower, compared to undoped titania. However,

23

when analysing the band gap values of C-doped coatings it should be considered that the band gap of rutile titanium dioxide is lower than that of anatase (3.0 eV compared to 3.2 eV for anatase [49]). As carbon incorporation into the titania lattice promotes rutile formation – all carbon-doped samples exhibited mixed phase structures, compared to the pure anatase structure of the undoped titania sample – therefore, some proportion of the decrease of the band gap value for C-doped films should be attributed to these phase transformations, rather than to narrowing of the intrinsic band gap due to the presence of carbon.

It is known that a higher surface area of the sample contributes to higher photocatalytic activity, as it increases the area of the contact between the photocatalyst and the pollutant. Nevertheless, in this case, regardless of carbon content, the surface area and surface roughness values of the samples were very similar, therefore the values of the photocatalytic activity could be compared directly.

It can be observed that the results of both methylene blue and stearic acid decomposition showed a similar trend; with C-doped samples being significantly more efficient both under UV and visible light, as compared to undoped TiO_2. Though the performance of undoped samples under visible light was fairly low for both pollutants, some low-level effect can be seen in the case of MB, which is probably due to the photobleaching phenomenon mentioned earlier. For both pollutants used, the photocatalytic performance of C-doped samples was of similar efficiency, with reaction constants for samples T25C100 – T30C200 being very close. This is probably explained by the fact that, according to the XPS analysis, the atomic percentage of carbon dopant in the titania lattice was very similar for samples T25C100, T30C100 and T35C100 (slightly higher for the C200 array), which is supposedly within the optimum dopant level. We suggest that the low photocatalytic activity of sample T35C200, despite the low value of its band gap and the atomic percent of C-dopant being close to the other C-doped samples, is related to the formation of carbonaceous species on the surface of the sample due to excessive amounts of carbon during the deposition process. Such species are often reported to form as a

result of excessive carbon doping, and though they increase the visible light absorption, they also lower the photocatalytic activity of samples by blocking the active sites and promoting faster electron-hole recombination [50]. Low value of average visible light transmittance, compared to the other samples of the array, confirms the initial suggestion.

It is generally accepted that the phenomenon of photoinduced hydrophilicity on titania surfaces originates from water adsorption on oxygen vacancies created by sub-band gap light irradiation [51]. While the morphology of the coating can have an impact on the wettability properties, it is known that values of surface roughness, R_a<0.5 μm, do not have a significant impact on the samples' wettability [52]. Therefore, wettability data of all the samples studied here can be directly compared. Despite the different intrinsic origins of the photocatalytic and superhydrophilic properties [53] and the fact that the photo-induced hydrophilic conversion does not necessarily indicate high efficacy in photodegradation of pollutants, in the case of titanium dioxide coatings the phenomenon of photoinduced hydrophilicity may be taken as indirect evidence of the photocatalytic properties of the film. Therefore, it is not surprising that in the WCA study the response of the undoped titania coatings to the irradiation was significantly lower under visible light, as compared to the C-doped coatings, as higher band gap values result in a significantly lower number of photogenerated species and hence a lower number of water molecules trapped on the surface of the photocatalyst. Similarly, under UV light irradiation, lower contact angle values were also observed for C-doped samples, due to the supposedly more efficient separation of photogenerated charge carriers and their extended lifetime, compared to undoped TiO_2.

Interestingly, the enhancement of the photocatalytic activity through C-doping via the reactive co-sputtering process followed a different trend, as compared to other methods of C incorporation (e.g. through the use of CO_2 [33]). It was readily observable that incorporation of carbon into the titania lattice occurred here by substituting some Ti atoms with C, while for the coatings deposited using CO_2, carbon tended to substitute both oxygen and titanium atoms. C-

doping of titania coatings via reactive co-sputtering resulted in a considerable improvement of photocatalytic activity against both model pollutants, in contrast to the coatings studied by earlier authors [33], where C-doping had a rather detrimental effect on the photocatalytic activity of the samples. Since both deposition techniques (reactive co-sputtering and the use of CO_2 as reactive gas) allowed the production of samples with comparable C content, but distinctively different properties, it is obvious that the position of carbon in the titania lattice is very important and influences the photocatalytic activity of the samples. However, the exact mechanism of activity enhancement observed for reactively co-sputtered coatings is not yet clear, and more work is currently in progress, including plasma physics studies and analysis of the lifetime of the photogenerated charge carriers.

Summarising all the above, low-level carbon doping results in enhancing UV- and introducing visible light activity, compared to undoped titania coatings deposited under identical conditions. This effect is supposedly a result of more efficient electron-hole separation, as well as band gap narrowing due to substitution of titanium atoms with carbon atoms. Overall, it can be concluded that reactive magnetron co-sputtering provides a simple, yet efficient route to the deposition of C-doped titania photocatalysts, however, further optimisation of deposition parameters is crucial in this case to maximise the coatings efficiency, as excessive carbon doping is shown to cease the photocatalytic activity.

5. Conclusion

The present work demonstrates that carbon doping is an efficient method of enhancing the photocatalytic activity of magnetron sputtered TiO_2 coatings. Carbon-doped titanium dioxide coatings were produced by reactive magnetron co-sputtering of Ti and C targets in an Ar / O_2 atmosphere, by varying both oxygen flow set point and power applied to the carbon target, and were compared to undoped titania coatings deposited under matching conditions. The content of carbon in the coatings varied from ca. 5 to 9 at.%, while the atomic percentage of carbon atoms incorporated in place of titanium atoms varied from ca. 0.5 to 1.8 at. %. The presence of carbon

has been found to reduce thermal stability of the anatase phase and lower the rutile formation temperature; all of C-doped samples were found to be a mixture of titania phases. Noticeable narrowing of the band gap was recorded for C-doped films, compared to undoped titanium dioxide. A series of tests was conducted to study the photocatalytic properties of the samples, including methylene blue dye and stearic acid decomposition, as well as photoinduced hydrophilicity measurements under UV and visible light sources. The results of all three tests showed similar trends, with the photocatalytic response of the C-doped titania coatings being higher under either of the light sources used. The latter suggested that carbon incorporation increased visible light activity, as well as extended the lifetime of photogenerated charge carriers. However, excessive carbon doping resulted in blockage of active sites and loss of photocatalytic properties.

Acknowledgements

References

[1] A. Fujishima, X. Zhang, Titanium dioxide photocatalysis: present situation and future approaches, Comptes Rendus Chimie 9(5-6) (2006) 750-760.

[2] M. Pelaez, N.T. Nolan, S.C. Pillai, M.K. Seery, P. Falaras, A.G. Kontos, P.S.M. Dunlop, J.W.J. Hamilton, J.A. Byrne, K. O'Shea, M.H. Entezari, D.D. Dionysiou, A review on the visible light active titanium dioxide photocatalysts for environmental applications, Applied Catalysis B: Environmental 125(0) (2012) 331-349.

[3] V. Shapovalov, Nanopowders and films of titanium oxide for photocatalysis: A review, Glass Physics and Chemistry 36(2) (2010) 121-157.

[4] S. Rehman, R. Ullah, A.M. Butt, N.D. Gohar, Strategies of making TiO_2 and ZnO visible light active, Journal of Hazardous Materials 170(2-3) (2009) 560-569.

[5] M. Ratova, P. Kelly, G. West, L. Tosheva, A Novel Technique for the Deposition of Bismuth Tungstate onto Titania Nanoparticulates for Enhancing the Visible Light Photocatalytic Activity, Coatings 6(3) (2016) 29.

[6] M. Ratova, P.J. Kelly, G.T. West, L. Tosheva, M. Edge, Reactive magnetron sputtering deposition of bismuth tungstate onto titania nanoparticles for enhancing visible light photocatalytic activity, Applied Surface Science 392 (2017) 590-597.

[7] M. Ratova, P.J. Kelly, G.T. West, I. Iordanova, Enhanced properties of magnetron sputtered photocatalytic coatings via transition metal doping, Surface and Coatings Technology 228, Supplement 1(0) (2013) S544-S549.

[8] M. Ratova, G. West, P. Kelly, Optimization Studies of Photocatalytic Tungsten-Doped Titania Coatings Deposited by Reactive Magnetron Co-Sputtering, Coatings 3(4) (2013) 194-207.

[9] M. Ratova, G.T. West, P.J. Kelly, X. Xia, Y. Gao, Synergistic effect of doping with nitrogen and molybdenum on the photocatalytic properties of thin titania films, Vacuum 114(0) (2015) 205-212.

[10] M.-C. Wang, H.-J. Lin, C.-H. Wang, H.-C. Wu, Effects of annealing temperature on the photocatalytic activity of N-doped TiO_2 thin films, Ceramics International 38(1) (2012) 195-200.

[11] R. Asahi, T. Morikawa, T. Ohwaki, K. Aoki, Y. Taga, Visible-Light Photocatalysis in Nitrogen-Doped Titanium Oxides, Science 293(5528) (2001) 269-271.

[12] M.V. Dozzi, E. Selli, Doping TiO_2 with p-block elements: Effects on photocatalytic activity, Journal of Photochemistry and Photobiology C: Photochemistry Reviews 14(0) (2013) 13-28.

[13] C.J. Tavares, S.M. Marques, T. Viseu, V. Teixeira, J.O. Carneiro, E. Alves, N.P. Barradas, F. Munnik, T. Girardeau, J.P. Riviere, Enhancement in the photocatalytic nature of nitrogen-

doped PVD-grown titanium dioxide thin films, Journal of Applied Physics 106(11) (2009) 113535-113535-8.

[14] M.M. Joshi, N.K. Labhsetwar, P.A. Mangrulkar, S.N. Tijare, S.P. Kamble, S.S. Rayalu, Visible light induced photoreduction of methyl orange by N-doped mesoporous titania, Applied Catalysis A: General 357(1) (2009) 26-33.

[15] A. Morawski, M. Janus, B. Tryba, M. Toyoda, T. Tsumura, M. Inagaki, Carbon Modified TiO_2 Photocatalysts for Water Purification, 2009.

[16] Y.-T. Lin, C.-H. Weng, Y.-H. Lin, C.-C. Shiesh, F.-Y. Chen, Effect of C content and calcination temperature on the photocatalytic activity of C-doped TiO_2 catalyst, Separation and Purification Technology 116 (2013) 114-123.

[17] A. Zaleska, J.W. Sobczak, E. Grabowska, J. Hupka, Preparation and photocatalytic activity of boron-modified TiO_2 under UV and visible light, Applied Catalysis B: Environmental 78(1) (2008) 92-100.

[18] S. Liu, X. Chen, A visible light response TiO_2 photocatalyst realized by cationic S-doping and its application for phenol degradation, Journal of Hazardous Materials 152(1) (2008) 48-55.

[19] K. Elghniji, J. Soro, S. Rossignol, M. Ksibi, A simple route for the preparation of P-modified TiO_2: Effect of phosphorus on thermal stability and photocatalytic activity, Journal of the Taiwan Institute of Chemical Engineers 43(1) (2012) 132-139.

[20] K.-R. Wu, C.-H. Hung, Characterization of N,C-codoped TiO_2 films prepared by reactive DC magnetron sputtering, Applied Surface Science 256(5) (2009) 1595-1603.

[21] M. Rahman, B.H.Q. Dang, K. McDonnell, J.M.D. MacElroy, D.P. Dowling, Effect of Doping (C or N) and Co-Doping (C plus N) on the Photoactive Properties of Magnetron Sputtered Titania Coatings for the Application of Solar Water-Splitting, Journal of Nanoscience and Nanotechnology 12(6) (2012) 4729-4735.

[22] H. Liu, Z. Lu, l. Yue, J. Liu, Z. Gan, C. Shu, T. Zhang, J. Shi, R. Xiong, (Mo+N) codoped TiO_2 for enhanced visible-light photoactivity, Applied Surface Science 257(22) (2011) 9355-9361.

[23] X. Li, Y. Liu, P. Yang, Y. Shi, Visible light-driven photocatalysis of W, N co-doped TiO_2, Particuology 11(6) (2013) 732-736.

[24] C. Xie, S. Yang, B. Li, H. Wang, J.-W. Shi, G. Li, C. Niu, C-doped mesoporous anatase TiO_2 comprising 10 nm crystallites, Journal of Colloid and Interface Science 476 (2016) 1-8.

[25] J. Jia, D. Li, J. Wan, X. Yu, Characterization and mechanism analysis of graphite/C-doped TiO_2 composite for enhanced photocatalytic performance, Journal of Industrial and Engineering Chemistry 33 (2016) 162-169.

[26] A. Bai, W. Liang, G. Zheng, J. Xue, Preparation and enhanced daylight-induced photo-catalytic activity of transparent C-Doped TiO_2 thin films, J. Wuhan Univ. Technol.-Mat. Sci. Edit. 25(5) (2010) 738-742.

[27] J. Zhang, G.-F. Huang, D. Li, B.-X. Zhou, S. Chang, A. Pan, W.-Q. Huang, Facile route to fabricate carbon-doped TiO_2 nanoparticles and its mechanism of enhanced visible light photocatalytic activity, Applied Physics A 122(12) (2016) 994.

[28] P.J. Kelly, G.T. West, M. Ratova, L. Fisher, S. Ostovarpour, J. Verran, Structural Formation and Photocatalytic Activity of Magnetron Sputtered Titania and Doped-Titania Coatings, Molecules 19(10) (2014) 16327-16348.

[29] Y.N. Kok, P.J. Kelly, Properties of Pulsed Magnetron Sputtered TiO_2 Coatings Grown under Different Magnetron Configurations and Power Deliver Modes, Plasma Processes and Polymers 4(S1) (2007) S299-S304.

[30] R.D. Arnell, P.J. Kelly, J.W. Bradley, Recent developments in pulsed magnetron sputtering, Surface and Coatings Technology 188–189(0) (2004) 158-163.

[31] D. Xie, F. Wen, W. Yang, X. Li, Y.X. Leng, G. Wan, H. Sun, N. Huang, Carbon-Doped Titanium Oxide Films by DC Reactive Magnetron Sputtering Using CO_2 and O_2 as Reactive Gas, 2014.

[32] F. Wen, C. Zhang, D. Xie, H. Sun, Y.X. Leng, Research of composition and photocatalytic property of carbon-doped Ti-O films prepared by R-MS using CO_2 gas resource, Nuclear

Instruments & Methods in Physics Research Section B-Beam Interactions with Materials and Atoms 307 (2013) 381-384.

[33] R. Klaysri, M. Ratova, P. Praserthdam, P. Kelly, Deposition of Visible Light-Active C-Doped Titania Films via Magnetron Sputtering Using CO_2 as a Source of Carbon, Nanomaterials 7(5) (2017) 113.

[34] H. Irie, S. Washizuka, K. Hashimoto, Hydrophilicity on carbon-doped TiO_2 thin films under visible light, Thin Solid Films 510(1-2) (2006) 21-25.

[35] S.S. Pradhan, S. Sahoo, S.K. Pradhan, Influence of annealing temperature on the structural, mechanical and wetting property of TiO_2 films deposited by RF magnetron sputtering, Thin Solid Films 518(23) (2010) 6904-6908.

[36] L. Zhu, X.L. Cui, J. Shen, X.L. Yang, Z.J. Zhang, Visible light photoelectrochemical response of carbon-doped TiO_2 thin films prepared by DC reactive magnetron sputtering, Acta Physico-Chimica Sinica 23(11) (2007) 1662-1666.

[37] M. Ratova, P. Kelly, G. West, X. Xia, Y. Gao, Deposition of Visible Light Active Photocatalytic Bismuth Molybdate Thin Films by Reactive Magnetron Sputtering, Materials 9(2) (2016) 67.

[38] J. Tauc, R. Grigorovici, A. Vancu, Optical Properties and Electronic Structure of Amorphous Germanium, physica status solidi (b) 15(2) (1966) 627-637.

[39] M. Rochkind, S. Pasternak, Y. Paz, Using Dyes for Evaluating Photocatalytic Properties: A Critical Review, Molecules 20(1) (2015) 88-110.

[40] A. Mills, M. McFarlane, Current and possible future methods of assessing the activities of photocatalyst films, Catalysis Today 129(1–2) (2007) 22-28.

[41] R. Quesada-Cabrera, A. Mills, C. O'Rourke, Action spectra of P25 TiO_2 and a visible light absorbing, carbon-modified titania in the photocatalytic degradation of stearic acid, Applied Catalysis B: Environmental 150-151(Supplement C) (2014) 338-344.

[42] A. Fujishima, K. Hashimoto, W. T., TiO_2 Photocatalysis: Fundamentals and Applications, BKC, Tokyo, Japan1999.

[43] A. Rampaul, I.P. Parkin, S.A. O'Neill, J. DeSouza, A. Mills, N. Elliott, Titania and tungsten doped titania thin films on glass; active photocatalysts, Polyhedron 22(1) (2003) 35-44.

[44] Y. Zhang, Z. Zhao, J. Chen, L. Cheng, J. Chang, W. Sheng, C. Hu, S. Cao, C-doped hollow TiO_2 spheres: in situ synthesis, controlled shell thickness, and superior visible-light photocatalytic activity, Applied Catalysis B: Environmental 165 (2015) 715-722.

[45] ISO10678, Fine ceramics, advanced technical ceramics - determination of photocatalytic activity of surfaces in an aqueous medium by degradation of methylene blue, ISO, Geneva, 2010.

[46] A. Mills, C. Hill, P.K.J. Robertson, Overview of the current ISO tests for photocatalytic materials, Journal of Photochemistry and Photobiology A: Chemistry 237(0) (2012) 7-23.

[47] M. Ratova, G.T. West, P.J. Kelly, Optimisation of HiPIMS photocatalytic titania coatings for low temperature deposition, Surface and Coatings Technology 250(0) (2014) 7-13.

[48] R. Su, R. Bechstein, L. Sø, R.T. Vang, M. Sillassen, B. Esbjörnsson, A. Palmqvist, F. Besenbacher, How the Anatase-to-Rutile Ratio Influences the Photoreactivity of TiO_2, The Journal of Physical Chemistry C 115(49) (2011) 24287-24292.

[49] E.M. Moser, S. Chappuis, J. Olleros, Production of photocatalytically active titania layers: A comparison of plasma processes and coating properties, Surface & Coatings Technology 227 (2013) 2-9.

[50] C. Xu, R. Killmeyer, M.L. Gray, S.U.M. Khan, Photocatalytic effect of carbon-modified n-TiO_2 nanoparticles under visible light illumination, Applied Catalysis B: Environmental 64(3) (2006) 312-317.

[51] K.G. Grigorov, I.C. Oliveira, H.S. Maciel, M. Massi, M.S. Oliveira, J. Amorim, C.A. Cunha, Optical and morphological properties of N-doped TiO_2 thin films, Surface Science 605(7) (2011) 775-782.

[52] A. Rudawska, E.b. Jacniacka, Analysis for determining surface free energy uncertainty by the Owens-Wendt method, International Journal of Adhesion and Adhesives 29(4) (2009) 451-457.

[53] D. Luca, D. Mardare, F. Iacomi, C.M. Teodorescu, Increasing surface hydrophilicity of titania thin films by doping, Applied Surface Science 252(18) (2006) 6122-6126.